

Efficient cathodoluminescence of monolayer transitional metal dichalcogenides in a van der Waals heterostructure

Shoujun Zheng¹, Jinkyu So², Fucui Liu³, Zheng Liu³, Nikolay Zheludev^{1,*}, and Hong Jin Fan^{1,2,*}

¹*Centre for Disruptive Photonic Technologies, Nanyang Technological University, 637371, Singapore*

²*Division of Physics and Applied Physics, School of Physical and Mathematical Sciences, Nanyang Technological University, 637371, Singapore*

³*School of Materials Science and Engineering, Nanyang Technological University, 639798, Singapore*

S. Zheng and J. So contributed equally to this work.

**Corresponding authors. Emails: NZheludev@ntu.edu.sg (N.Z.); fanhj@ntu.edu.sg (H.J.F.)*

Abstract: Monolayer two-dimensional transitional metal dichalcogenides, such as MoS₂, WS₂ and WSe₂, are direct band gap semiconductors with large exciton binding energy. They attract growing attentions for opto-electronic applications including solar cells, photo-detectors, light-emitting diodes and photo-transistors, capacitive energy storage, photodynamic cancer therapy and sensing on flexible platforms. While light-induced luminescence has been widely studied, luminescence induced by injection of free electrons could promise another important applications of these new materials. However, cathodoluminescence is inefficient due to the low cross-section of the electron-hole creating process in the monolayers. Here for the first time we show that cathodoluminescence of monolayer chalcogenide semiconductors can be evidently observed in a van der Waals heterostructure when the monolayer semiconductor is sandwiched between layers of hexagonal boron nitride (hBN) with higher energy gap. The emission intensity shows a strong dependence on the thicknesses of surrounding layers and the enhancement factor is more than 1000 folds. Strain-induced exciton peak shift in the suspended heterostructure is also investigated by the cathodoluminescence spectroscopy. Our results demonstrate that MoS₂, WS₂ and WSe₂ could be promising cathodoluminescent materials for applications in single-photon emitters, high-energy particle detectors, transmission electron microscope displays, surface-conduction electron-emitter and field emission display technologies.

Keywords: transitional metal dichalcogenides; van der Waals heterostructures; cathodoluminescence; strain effect; 2D heterostructures

Introduction

Two-dimensional (2D) layered semiconductors, due to their weak interlayer van der Waals bonds, can be easily thinned down to atomic thickness by mechanical¹ and chemical² exfoliation methods, for example, graphene³ and hexagonal boron nitride (hBN)⁴. Monolayer transitional metal dichalcogenides with the formula of MX_2 (M=Mo, W; X=S, Se, Te) are a type of unique semiconductors with narrow direct band gaps, large exciton binding energies, high optoconductivity, and high photoelectrochemical activity. Moreover, due to the inversion symmetry breaking, monolayer MX_2 are widely employed for the study of valley polarization and spin–valley coupling^{5, 6}. Recently, van der Waals heterostructures, composed of different 2D materials with unique band alignment and interlayer coupling, attract growing attentions not only for fundamental new physics but also for many potential applications such as tunneling transistors^{7, 8, 9} and light-emitting diodes¹⁰.

Cathodoluminescence, photon emission excited by a high-energy electron beam, is widely applied in the analysis of mineral compositions¹¹, light emitting diodes^{12, 13}, surface plasmon mapping¹⁴. Compared to photoluminescence excited by light, cathodoluminescence offers a much higher excitation energy allowing the study of wide band gap materials including diamond¹⁵ and hexagonal boron nitride (hBN)^{16, 17}. Due to a small excitation hotspot cathodoluminescence has been extensively used to study nanostructures including hyper-spectral imaging of plasmonic gratings¹⁸, nanoparticles¹⁹, nano-antenna²⁰, quantum well^{21, 22}, three-dimensional nanoscale visualization of metal-dielectric nanoresonators²³ and nanoscale light sources^{24, 25}.

In atomic layers of MX_2 , it is challenging to detect the interband cathodoluminescence signal as the electron-hole creation cross section is extremely small. Moreover, the spatial distribution of electron-hole pairs at the interface, which is near the point of free-electron injection, is close to a 3D spherical shape of a few microns in diameter. Only a small fraction of recombination takes place in the top 2D material and most of them happen in the supporting slab. Indeed, so far only a few reports are available on cathodoluminescence study of 2D materials, including six atomic layer thick flakes of boron nitride.^{26, 27, 28} However, cathodoluminescence from monolayer MX_2 has not reported.

In this report we show that cathodoluminescence emissions from monolayer MX_2 (MoS_2 , WS_2 and WSe_2) can be enhanced and efficiently detected in a van der Waals heterostructure, in which the luminescent MX_2 layer is sandwiched between layers of hexagonal boron nitride (hBN) with higher energy gap (see schematics in Fig. 1a). Here the hBN/ MX_2 /hBN heterostructure can effectively increase

the recombination probability of electron-hole pairs in the monolayer MX_2 in such a way that a good fraction of the electrons and holes generated in the hBN layers diffuse to and then radiative recombine in the MX_2 layer, leading to significant enhancement of the emission, comparatively to an isolated layer (Fig. 1b).

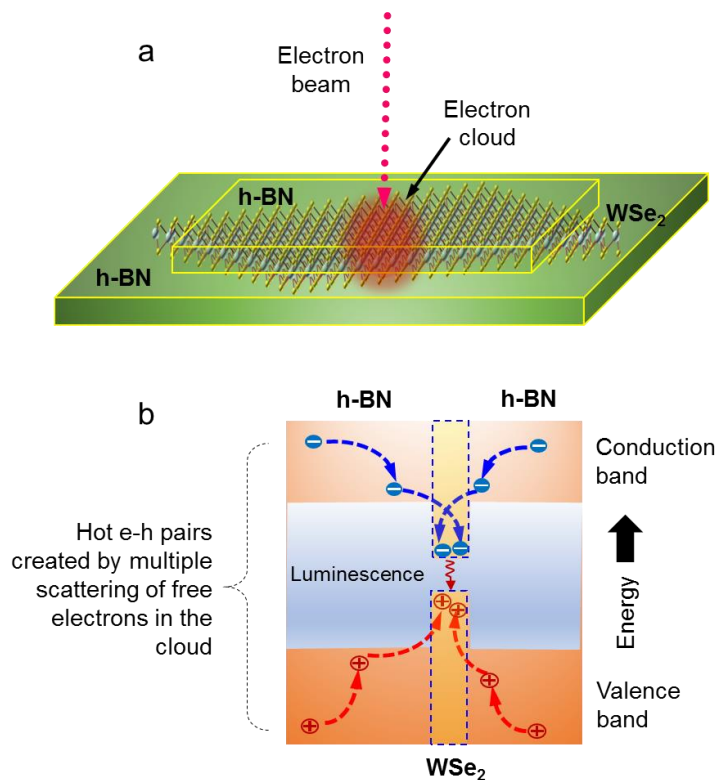


Figure 1 | (a) Illustration of cathodoluminescence in an hBN/ MX_2 /hBN van der Waals heterostructure. (b) Process of the generation, diffusion and recombination of e-h pairs. The minor number of e-h pairs generated in the MX_2 layer is ignored.

Cathodoluminescence of hBN/monolayer WSe_2 /hBN heterostructure

To fabricate the hBN/ MX_2 /hBN structure, we stacked the different layers one by one by the dry pick-up transfer method^{1, 29}. Firstly, an hBN flake was picked up by a polydimethylsiloxane (PDMS) film with a spincoated polyvinyl alcohol (PVA) layer. Then the hBN flake supported by the PDMS/PVA film was aligned to the monolayer WSe_2 flake to pick up it by the Van der Waals force (Fig. 2a). Next, the hBN/ WSe_2 heterostructure was aligned to a large and thick bottom hBN (thickness ~ 100 nm). Finally the PDMS/PVA film was removed (see details in the supporting materials and Fig. S1). Figure 2b shows the optical image of the prepared hBN/ WSe_2 /hBN heterostructure. Some bubbles generated during sample transfer process and enlarged when the sample was put into SEM vacuum chamber (see in Fig. S2a), which can be proved by atomic force microscopy topography image (indicated by the bright dots

in Fig. S2c). The thickness of the top hBN layer is around 4.2 nm. Furthermore, the monolayer WSe₂ is clearly identified by Raman mapping (Fig. S2b), in which the Raman intensities of the vibration mode A_{1g} are less affected by the top hBN layer.

When cathodoluminescence measurement was done to monolayer MX₂ on Si substrates or freestanding monolayer MX₂, the emissions are too weak to be observable. However, strong emissions from the monolayer WSe₂ can be observed in the hBN/WSe₂/hBN van der Waals heterostructure (acceleration voltage of 5 keV, beam current of 36.2 nA). Cathodoluminescence mapping clearly shows the giant enhancement of the emission intensity in the hBN/WSe₂/hBN region (indicated by red color in Fig. 2c). The cathodoluminescence signal was only present in the hBN/WSe₂/hBN region (indicated by point 1), but absent in the WSe₂ region without the top hBN layer (point 2). Therefore, both the top and bottom hBN layer are key factors to cathodoluminescence emission of monolayer WSe₂. The cathodoluminescence emission peak around 1.572 eV corresponds to the excitonic energy of the monolayer WSe₂ (Fig. 2d). This cathodoluminescence emission peak is consistent to the photoluminescence (PL) emission peak, but with a small redshift of 16.8 meV. The disalignment between CL and PL peak position may be due to the local heating effect by the e-beam, which is consistent to the well-known temperature-induced semiconductor band gap shrinkage³⁰. Similar redshifts were also observed from other MX₂ samples in the heterostructure. Moreover, the cathodoluminescence intensity is proportional to the electron beam currents (see Fig. S2e and inset) and unresolvable when the beam current is below 1.9 nA.

We also investigated the time-resolved cathodoluminescence by a streak camera at room temperature. The time-resolved spectrum (inset of Fig. 2d) was well fitted with a double exponential decay function of $Ae^{-t/\tau_1} + Be^{-t/\tau_2}$. The decay times of τ_1 and τ_2 are 36.8 and 369.9 ps, respectively. The intrinsic exciton lifetime of the monolayer MX₂ is predicted to be 0.1~1 ps according to theoretical calculations^{31, 32}. Several experiments show that the exciton lifetime can reach several ps at the low temperature of a few K^{33, 34}. However, the lifetime increases at high temperatures. The effective decay lifetime at a given temperature T is given by $\tau_{rad}^{eff} = \frac{3k_B T}{2E_0} \tau_{rad}^0$ where τ_{rad}^0 is the intrinsic exciton lifetime at 0 K, $k_B T$ is the thermal energy, E_0 is the kinetic energy of the exciton. According to this equation, the effective decay lifetime of the exciton becomes longer at room temperature, which even reaches hundreds ps to several ns³³. As the lifetime of the trion is generally shorter than the one of exciton^{35, 36}, the decay times

of 36.8 and 369.9 ps may be related to the trion and exciton, respectively.

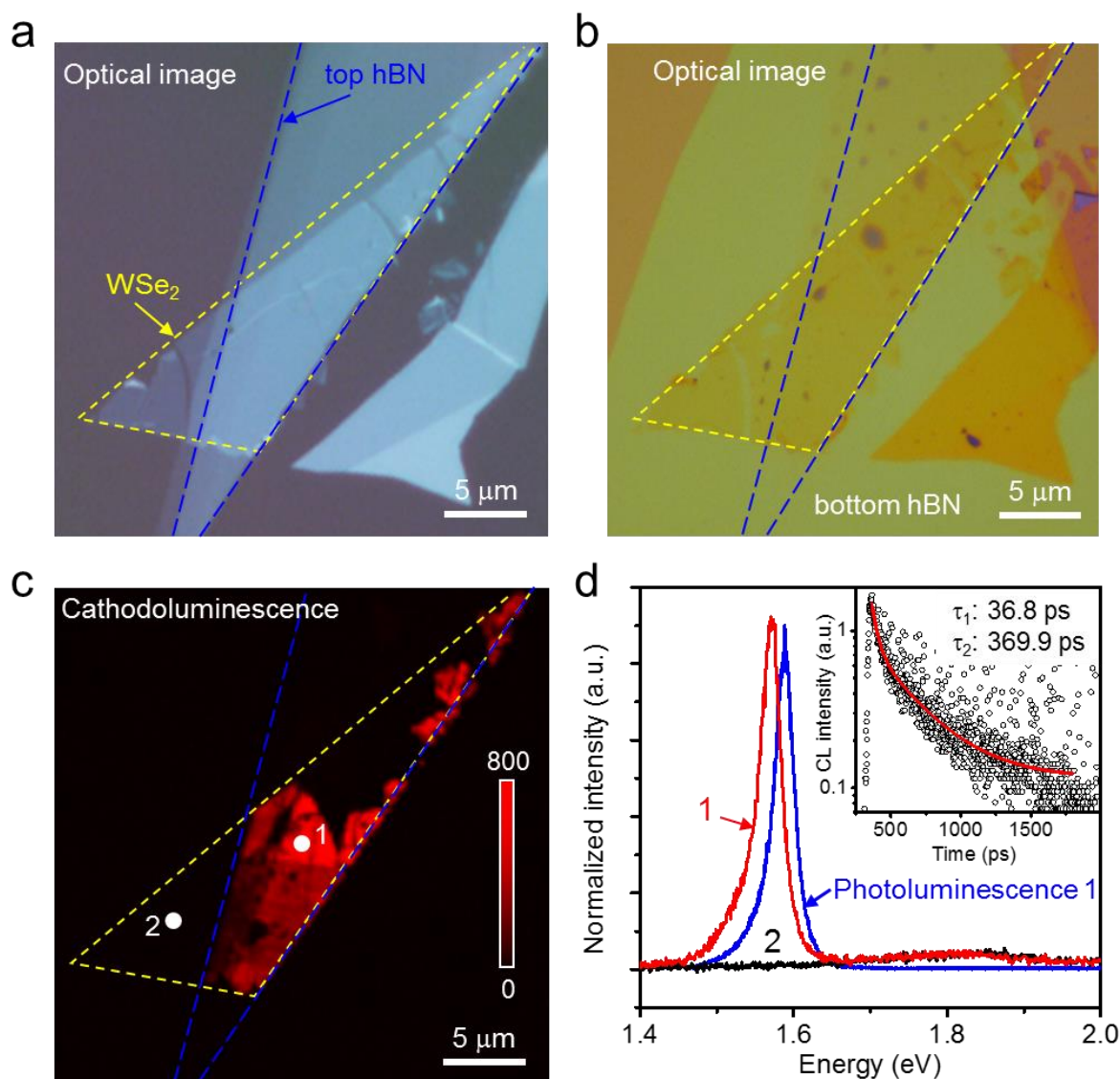


Figure 2 | Cathodoluminescence of the monolayer WSe₂. (a) Optical image of the hBN/WSe₂ structure on a PDMS/PVA film before the last transfer step. The top hBN and WSe₂ layers can be easily seen. (b) Optical image of the prepared hBN/WSe₂/hBN heterostructure. (c) Cathodoluminescence intensity mapping of the hBN/WSe₂/hBN heterostructures. The strong emission is indicated by the red color. 1: hBN/WSe₂/hBN part. 2: WSe₂/hBN part without the top hBN layer. (d) Cathodoluminescence and photoluminescence spectra. The numbers correspond to the two points in (c). Inset is the time-resolved cathodoluminescence spectrum recorded at room temperature.

The dependence of cathodoluminescence intensity on hBN thickness

It is found that the emission intensity is strongly dependent on the thicknesses of both top and bottom hBN layers. We fabricated an hBN/WSe₂/hBN sample with a flat bottom hBN layer of 165.3 nm and a top hBN layer with different thickness regions of 3.5, 11.8, and 23.0 nm (see more details in Fig. S3a-

c). The cathodoluminescence mapping shows clearly the intensity difference between the three thickness regions; highest at the region of 23.0 nm and weakest at the one of 3.5 nm. This can be clearly seen from the cathodoluminescence spectra selected from the three regions (Fig. 3a). Each spectrum is the average of 20 points selected from the corresponding region to eliminate intensity inhomogeneity. The dependence of integrated intensity on top hBN thickness is plotted in Fig. 3b, which is nearly a linear relationship. Furthermore, we found that the intensity has a similar dependence on the thickness of the bottom hBN layer. We prepared another hBN/WSe₂/hBN sample with a flat top hBN layer (20 nm thick), and a bottom hBN layer of four thickness regions of 12.1, 21.6, 36.7, 48.3 nm (see details in Fig. S3d-f). The cathodoluminescence mapping can also be identified with four parts corresponding to the four thickness regions. The average spectra selected from each regions also attest this intensity difference (Fig. 3c). The difference in peak positions in Fig. 3 may be related to spatial-dependent strain and/or heterostructure inhomogeneity. Similar to above where the top hBN layer thickness is varied, the plot of cathodoluminescence intensity as a function of the thickness of the bottom hBN layer shows a nearly linear relationship (Fig 3d). We have also conducted similar tests on other heterostructures and obtained similar trend. Such a strong thickness dependence concords with our notion that the e-h pairs for recombination originate mainly from the hBN layers, in which a larger thickness corresponds to a higher excitation volume. According to calculations, the diffusion lengths for electrons and holes in hBN are in the μm range,³⁷ so the e-h pairs generated in both top and bottom hBN layers in the heterostructure can diffuse to the middle MX₂ layer before recombination. Therefore, it is reasonable that cathodoluminescence intensity has a strong dependence on the thickness of the hBN layers.

The question is, why both top and bottom hBN layers are necessary for evident cathodoluminescence emission. In our configuration, strong emission from WSe₂ requires that the generated e-h pairs can efficiently diffuse to and be trapped at the interface between the two hBN layers. Because of the potential well, the carriers are transferred to the middle MX₂ which is the recombination center, leading to evident luminescence emission. In case of a single top or bottom hBN layer, the generated e-h pairs are not efficiently confined at the surface of the hBN layer even with a monolayer MX₂. Therefore, the strong cathodoluminescence due to WSe₂ band gap emission is attributed to the both increased excitation volume and efficient interface confinement of e-h pairs in the sandwich configuration. The enhancement factor is more than 1000 when the thicknesses of both top and bottom hBN layers are 19.8

and 123.9 nm (Fig. S4). Finally, it is noteworthy that the bottom hBN layer cannot be replaced by the amorphous SiO₂ substrate, as the latter does not provide a van der Waals contact.

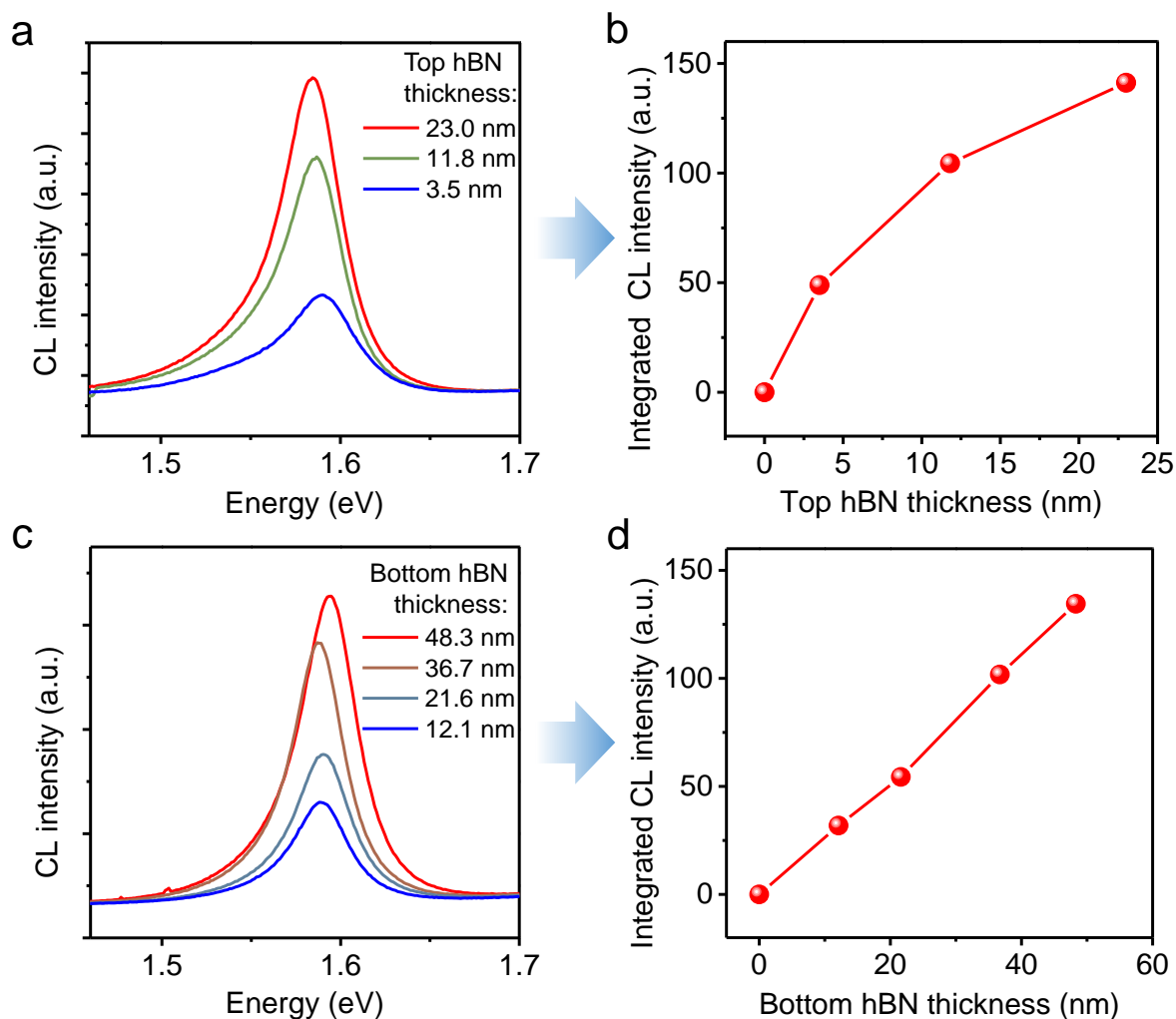


Fig. 3 | Effects of hBN layers thickness on cathodoluminescence intensity. (a) Spectra collected from three regions of different top hBN thicknesses. Each spectrum is the average of 20 points selected from the same thickness region. (b) The plot of integrated intensity versus the thickness of the top hBN layer. (c) Averaged spectra from the four regions of different bottom hBN thicknesses. (d) Plot of integrated intensity versus the bottom hBN layer thickness.

Effect of strain

Cathodoluminescence spectroscopy is also powerful in revealing spatial-resolved strain effect in 2D semiconductors. It is known that the band gap shift in MX₂ is sensitive to the strain, as evidenced in both theoretical calculations³⁸ and experiments^{39, 40, 41}. We investigated the strain-induced peak shift of the monolayer WSe₂ by suspending the hBN/WSe₂/hBN heterostructure sample on holes made on the Si substrate. Array of holes were fabricated by a focused ion beam with diameter of 1 and 2 μm, so that

part of the sample is suspended (Fig. S5). Interestingly, the emission intensity of hBN/WSe₂/hBN suspended on the hole is much stronger than the part laid on the substrate at room temperature (Fig. 4a). By cooling down the sample, we can identify the exciton and trion peak positions clearly from the spectra. Position-dependent spectra at 10 K (Fig. 4b and 4c) clearly shows that the excitonic peak redshift with a maximum shift of 12.1 meV from the edge to the center of the hole due to strain.

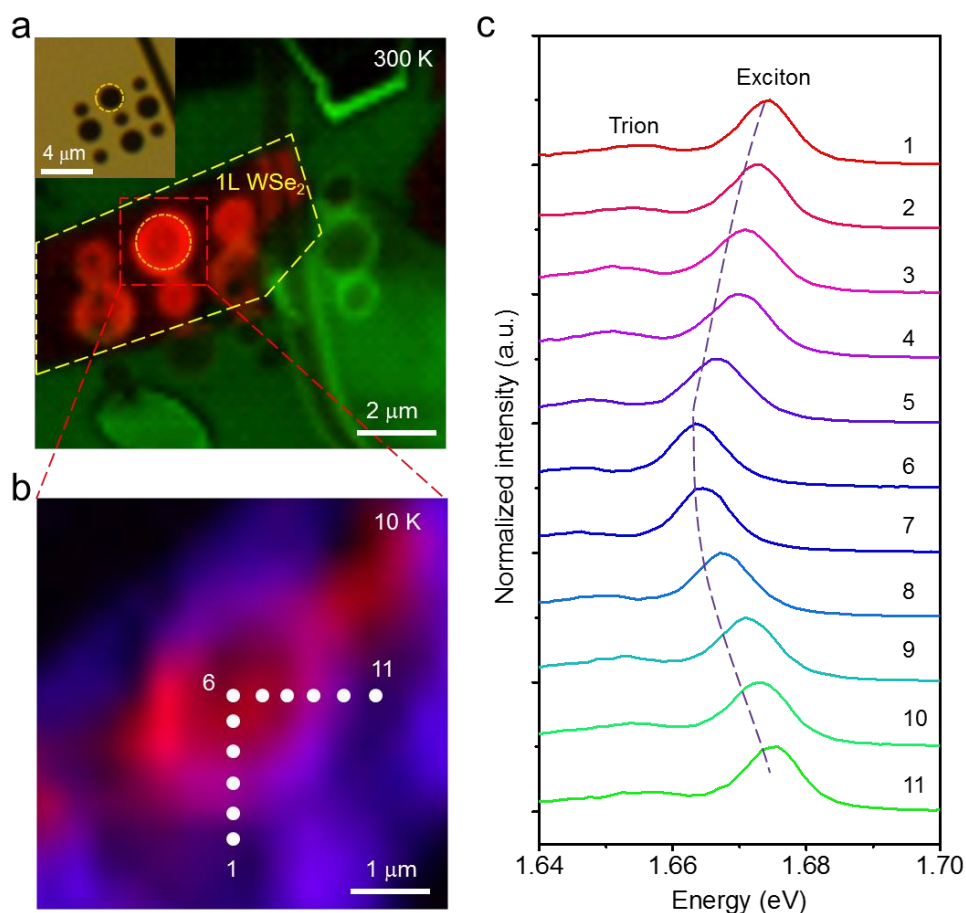


Figure 4 | Strain effect. (a) Cathodoluminescence mapping of the hBN/WSe₂/hBN sample at room temperature. Parts of the samples are suspended on focused-ion beam fabricated holes on the substrate. Inset is the Si substrate with holes before transfer. (b) Enlarged cathodoluminescence mapping at 10 K around a hole. (c) Position-dependent spectra taken from a series of points in (b).

In addition to the strain due to suspension, strain in the thin heterostructures is also inevitably introduced during the transfer process. Such inhomogeneous local strain in the heterostructures is also detectable by cathodoluminescence spectroscopy. Indeed two energy domains were observed from the hBN/WSe₂/hBN (indicated by purple and green colors in Fig. S6a) sample in terms of the exciton peak position at 77 K. From the CL spectra from selected points (Fig. S6b), two emission peaks can be

resolved at both point A and B. The two peaks correspond to the emissions of neutral excitons and trions (charged excitons)⁴². However, the peak positions of excitons and trions at point A are 1.640 and 1.614 eV, respectively, while 1.657 and 1.623 eV at point B. The peak position difference between point A and B in the heterostructure may be caused by strain, which is possibly generated during the transfer process (e.g., bubbles).

Temperature dependent cathodoluminescence spectra of the point B were plotted in Fig. S5c. The peak positions of both excitons and trions are fitted (Fig. S5d) according to the semiempirical semiconductor band gap equation^{30, 43} of $E_g(T) = E_g(0) - S\hbar\omega \left[\coth\left(\frac{\hbar\omega}{2kT}\right) - 1 \right]$, where $E_g(0)$ is the excitonic energy at 0 K, S is a dimensionless coupling constant and $\hbar\omega$ is an average phonon energy. From the fitting curves, we extract $E_g(0)$ of the exciton and trion of the monolayer WSe₂ to be 1.6652 and 1.6344 eV, respectively. So, the binding energy of the trion is calculated to be 30.8 meV which is consistent with the previous report (30 meV)³².

Cathodoluminescence of other monolayer semiconductors

In addition to WSe₂, we also performed cathodoluminescence experiments to monolayer WS₂ and MoS₂ in a van der Waals heterostructure (sandwiched by two hBN layers). The emission peak position from the WS₂ heterostructure locates at 1.933 eV (Fig. 5a) and that from the MoS₂ in heterostructure at 1.831 eV (Fig. 5b). The emission peak positions of both two heterostructures redshift with respect to their photoluminescence peak positions, similar to the case of hBN/WSe₂/hBN. Cathodoluminescence mapping is inhomogeneous at the MoS₂ sample which is most likely due to poor interface contact. Therefore, sandwiching monolayer MX₂ into two hBN layers is a universal approach to study cathodoluminescence emissions of monolayer MX₂.

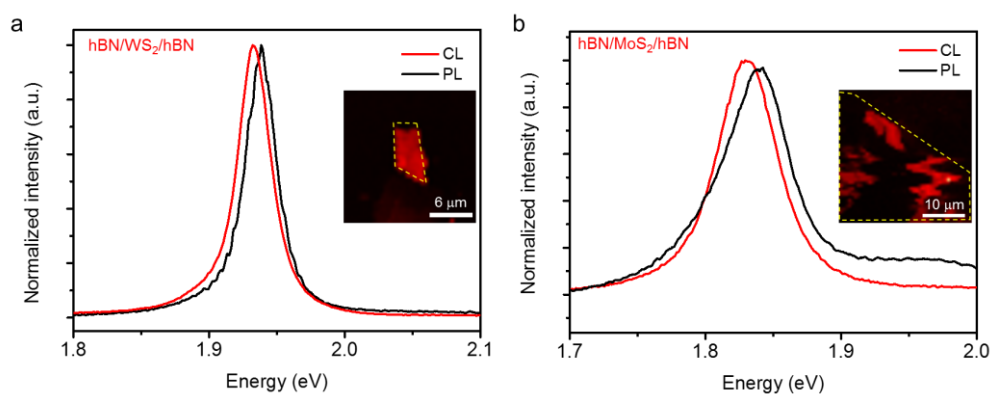


Figure 5 | Cathodoluminescence of monolayer WS₂ and MoS₂. (a) CL and PL spectra of the monolayer WS₂ in

the top-hBN (7.5 nm)/WS₂/bottom-hBN (299.4 nm). (b) CL and PL spectra of the monolayer MoS₂ in the top-hBN (13.5 nm)/MoS₂/bottom-hBN (168.6 nm). Insets are the corresponding cathodoluminescence intensity mappings. Yellow lines guide the shapes of monolayer TMDs in the van der Waals heterostructures.

In summary, for the first time we have obtained evident cathodoluminescence emission from monolayer MX₂, including WSe₂, MoS₂ and WS₂, via a van der Waals configuration. In the hBN/MX₂/hBN heterostructure, electron beam induced e-h pairs can transfer to and be trapped in the middle MX₂ layer, leading to increased recombination probability within the MX₂ layer. Moreover, we demonstrate that cathodoluminescence spectroscopy can be applied to study the strain-induced excitonic peak shift in monolayer MX₂. Because of its high spatial resolution and high beam energy, our demonstration makes cathodoluminescence spectroscopy a powerful technique to the study of 2D materials in various forms such as alloy, heterostructures or defects. The 2D monolayer-based heterostructure may promise potential applications in single-photon emitters, surface-conduction electron-emitter and field emission display technologies.

Methods

Fabrication of hBN/MX₂/hBN structures. Monolayer MX₂ and hBN layers were exfoliated on Si/SiO₂ wafers by scotch tapes and identified by a Nikon optical microscope. Top hBN layer and MX₂ layer were picked up by a PDMS/PVA film one by one, then aligned and put on the bottom hBN layer. PDMS/PVA film can be removed by slow detachment which may cause loose interface contact, or immersing in water (See details in the supporting materials). The holes on the Silicon substrate were fabricated by a focused ion beam (FEI Helios NanoLab) in 1~2 μm diameter and 1 μm depth.

AFM, Raman and photoluminescence characterization. The thicknesses of hBN layers were measured using a Cypher ES scanning probe microscopy. Raman and PL spectra were recorded from a Witec confocal Raman spectrum with an excitation wavelength of 532 nm under 100X objective.

Cathodoluminescence measurement. We used a commercial Cathodoluminescence Microscope (Attolight Allalin 4027 Chronos) with an accelerating voltage of 5 kV, a beam current of 36.2 nA, and an exposure time of 50 ms for most spectra (for beam current dependent spectra, the exposure time was 10 ms). Samples were loaded into the chamber under ultra-high vacuum (<10⁻⁵ Pa) and the emissions were collected by a UV-VIS spectrometer in the range of 180 - 1100 nm. Low-temperature spectra were collected by cooling down the sample using liquid nitrogen (78 K) and helium (10 K). For time-resolved spectra, a pulsed laser of 300 fs was used to generate electron pulse of around 5 ps and emission signals were collected by a streak camera with the range of 200 -850 nm.

Reference:

1. Castellanos-Gomez A, Buscema M, Molenaar R, Singh V, Janssen L, van der Zant HSJ, Steele GA. Deterministic transfer of two-dimensional materials by all-dry viscoelastic stamping. *2d Materials* **1**, 011002 (2014).

2. Chhowalla M, Shin HS, Eda G, Li LJ, Loh KP, Zhang H. The chemistry of two-dimensional layered transition metal dichalcogenide nanosheets. *Nat Chem* **5**, 263-275 (2013).
3. Novoselov KS, Geim AK, Morozov SV, Jiang D, Zhang Y, Dubonos SV, Grigorieva IV, Firsov AA. Electric field effect in atomically thin carbon films. *Science* **306**, 666-669 (2004).
4. Dean CR, Young AF, Meric I, Lee C, Wang L, Sorgenfrei S, Watanabe K, Taniguchi T, Kim P, Shepard K. Boron nitride substrates for high-quality graphene electronics. *Nat Nanotechnol* **5**, 722-726 (2010).
5. Zeng HL, Dai JF, Yao W, Xiao D, Cui XD. Valley polarization in MoS₂ monolayers by optical pumping. *Nat Nanotechnol* **7**, 490-493 (2012).
6. Shan WY, Lu HZ, Xiao D. Spin Hall effect in spin-valley coupled monolayers of transition metal dichalcogenides. *Phys Rev B* **88**, (2013).
7. Britnell L, Gorbachev R, Geim A, Ponomarenko L, Mishchenko A, Greenaway M, Fromhold T, Novoselov K, Eaves L. Resonant tunnelling and negative differential conductance in graphene transistors. *Nat Commun* **4**, 1794 (2013).
8. Nguyen L-N, Lan Y-W, Chen J-H, Chang T-R, Zhong Y-L, Jeng H-T, Li L-J, Chen C-D. Resonant tunneling through discrete quantum states in stacked atomic-layered MoS₂. *Nano Lett* **14**, 2381-2386 (2014).
9. Campbell PM, Tarasov A, Joiner CA, Ready WJ, Vogel EM. Enhanced Resonant Tunneling in Symmetric 2D Semiconductor Vertical Heterostructure Transistors. *Acs Nano* **9**, 5000-5008 (2015).
10. Withers F, Del Pozo-Zamudio O, Mishchenko A, Rooney AP, Gholinia A, Watanabe K, Taniguchi T, Haigh SJ, Geim AK, Tartakovskii AI, Novoselov KS. Light-emitting diodes by band-structure engineering in van der Waals heterostructures. *Nat Mater* **14**, 301-306 (2015).
11. Boggs S, Krinsley D. *Application of cathodoluminescence imaging to the study of sedimentary rocks*. Cambridge University Press (2006).
12. Chin AK, Zipfel CL, Mahajan S, Ermanis F, Digiuseppe MA. Cathodoluminescence Evaluation of Dark Spot Defects in InP/InGaAsP Light-Emitting-Diodes. *Appl Phys Lett* **41**, 555-557 (1982).
13. Griffiths JT, Zhang S, Rouet-Leduc B, Fu WY, Bao A, Zhu D, Wallis DJ, Howkins A, Boyd I, Stowe D, Kappers MJ, Humphreys CJ, Oliver RA. Nanocathodoluminescence Reveals Mitigation of the Stark Shift in InGaN Quantum Wells by Si Doping. *Nano Lett* **15**, 7639-7643 (2015).
14. Zhao M, Bosman M, Danesh M, Zeng M, Song P, Darma Y, Rusydi A, Lin H, Qiu CW, Loh KP. Visible Surface Plasmon Modes in Single Bi₂Te₃ Nanoplate. *Nano Lett* **15**, 8331-8335 (2015).
15. Ruf T, Cardona M, Sternschulte H, Wahl S, Thonke K, Sauer R, Pavone P, Anthony TR. Cathodoluminescence investigation of isotope effects in diamond. *Solid State Commun* **105**, 311-316 (1998).
16. Watanabe K, Taniguchi T, Kanda H. Direct-bandgap properties and evidence for ultraviolet lasing of hexagonal boron nitride single crystal. *Nat Mater* **3**, 404-409 (2004).
17. Arnaud B, Lebegue S, Rabiller P, Alouani M. Huge excitonic effects in layered hexagonal boron nitride. *Phys Rev Lett* **96**, 026402 (2006).
18. Bashevoy M, Jonsson F, MacDonald K, Chen Y, Zheludev N. Hyperspectral imaging of plasmonic nanostructures with nanoscale resolution. *Opt Express* **15**, 11313-11320 (2007).
19. Tikhomirov V, Adamo G, Nikolaenko A, Rodriguez V, Gredin P, Mortier M, Zheludev N, Moshchalkov V. Cathodo- and photoluminescence in Yb³⁺-Er³⁺ co-doped PbF₂ nanoparticles. *Opt Express* **18**, 8836-8846 (2010).
20. Denisyuk A, Adamo G, MacDonald K, Edgar J, Arnold M, Myroshnychenko V, Ford M, Garcia de Abajo FJ, Zheludev N. Transmitting hertzian optical nanoantenna with free-electron feed. *Nano Lett* **10**, 3250-

- 3252 (2010).
21. Xu J, Chen L, Yu L, Liang H, Zhang B, Lau KM. Cathodoluminescence study of InGaN/GaN quantum-well LED structures grown on a Si substrate. *Journal of Electronic Materials* **36**, 1144-1148 (2007).
 22. Priesol J, Satka A, Uherek F, Donoval D, Shields P, Allsopp DWE. Quantitative analysis of cathodoluminescence phenomena in InGaN/GaN QW by Monte Carlo method. *Applied Surface Science* **269**, 155-160 (2013).
 23. Atre AC, Brenny BJ, Coenen T, Garcia-Etxarri A, Polman A, Dionne JA. Nanoscale optical tomography with cathodoluminescence spectroscopy. *Nat Nanotechnol* **10**, 429-436 (2015).
 24. Adamo G, MacDonald KF, Fu Y, Wang C, Tsai D, de Abajo FG, Zheludev N. Light well: a tunable free-electron light source on a chip. *Phys Rev Lett* **103**, 113901 (2009).
 25. Li G, Clarke BP, So JK, MacDonald KF, Zheludev NI. Holographic free-electron light source. *Nat Commun* **7**, 13705 (2016).
 26. Bourrellier R, Amato M, Tizei LHG, Giorgetti C, Gloter A, Heggie MI, March K, Stephan O, Reining L, Kociak M, Zobelli A. Nanometric Resolved Luminescence in h-BN Flakes: Excitons and Stacking Order. *Acs Photonics* **1**, 857-862 (2014).
 27. Watanabe K, Taniguchi T, Niiyama T, Miya K, Taniguchi M. Far-ultraviolet plane-emission handheld device based on hexagonal boron nitride. *Nat Photonics* **3**, 591-594 (2009).
 28. Schue L, Berini B, Betz AC, Placais B, Ducastelle F, Barjon J, Loiseau A. Dimensionality effects on the luminescence properties of hBN. *Nanoscale* **8**, 6986-6993 (2016).
 29. Pizzocchero F, Gammelgaard L, Jessen BS, Caridad JM, Wang L, Hone J, Boggild P, Booth TJ. The hot pick-up technique for batch assembly of van der Waals heterostructures. *Nat Commun* **7**, 11894 (2016).
 30. O'Donnell K, Chen X. Temperature dependence of semiconductor band gaps. *Appl Phys Lett* **58**, 2924-2926 (1991).
 31. Palummo M, Bernardi M, Grossman JC. Exciton radiative lifetimes in two-dimensional transition metal dichalcogenides. *Nano Lett* **15**, 2794-2800 (2015).
 32. Wang H, Zhang C, Chan W, Manolatu C, Tiwari S, Rana F. Radiative lifetimes of excitons and trions in monolayers of the metal dichalcogenide MoS₂. *Phys Rev B* **93**, 045407 (2016).
 33. Robert C, Lagarde D, Cadiz F, Wang G, Lassagne B, Amand T, Balocchi A, Renucci P, Tongay S, Urbaszek B, Marie X. Exciton radiative lifetime in transition metal dichalcogenide monolayers. *Phys Rev B* **93**, 205423 (2016).
 34. Lagarde D, Bouet L, Marie X, Zhu C, Liu B, Amand T, Tan P, Urbaszek B. Carrier and polarization dynamics in monolayer MoS₂. *Physical review letters* **112**, 047401 (2014).
 35. Andreani LC, Tassone F, Bassani F. Radiative Lifetime of Free-Excitons in Quantum-Wells. *Solid State Commun* **77**, 641-645 (1991).
 36. Yan TF, Qiao XF, Liu XN, Tan PH, Zhang XH. Photoluminescence properties and exciton dynamics in monolayer WSe₂. *Appl Phys Lett* **105**, 101901 (2014).
 37. Maity A, Doan TC, Li J, Lin JY, Jiang HX. Realization of highly efficient hexagonal boron nitride neutron detectors. *Appl Phys Lett* **109**, 072101 (2016).
 38. Amin B, Kaloni TP, Schwingenschlogl U. Strain engineering of WS₂, WSe₂, and WTe₂. *Rsc Adv* **4**, 34561-34565 (2014).
 39. Castellanos-Gomez A, Roldán R, Cappelluti E, Buscema M, Guinea F, van der Zant HS, Steele GA. Local strain engineering in atomically thin MoS₂. *Nano Lett* **13**, 5361-5366 (2013).
 40. Conley HJ, Wang B, Ziegler JI, Haglund RF, Jr., Pantelides ST, Bolotin KI. Bandgap engineering of strained monolayer and bilayer MoS₂. *Nano Lett* **13**, 3626-3630 (2013).

41. Desai SB, Seol G, Kang JS, Fang H, Battaglia C, Kapadia R, Ager JW, Guo J, Javey A. Strain-Induced Indirect to Direct Bandgap Transition in Multi layer WSe₂. *Nano Lett* **14**, 4592-4597 (2014).
42. Wang G, Bouet L, Lagarde D, Vidal M, Balocchi A, Amand T, Marie X, Urbaszek B. Valley dynamics probed through charged and neutral exciton emission in monolayer WSe₂. *Phys Rev B* **90**, 075413 (2014).
43. Ross JS, Wu S, Yu H, Ghimire NJ, Jones AM, Aivazian G, Yan J, Mandrus DG, Xiao D, Yao W, Xu X. Electrical control of neutral and charged excitons in a monolayer semiconductor. *Nat Commun* **4**, 1474 (2013).

Acknowledgements

This work is supported by Singapore Ministry of Education Academic Research Fund Tier 3 (Grant No. MOE2011-T3-1-005) and the Singapore National Research Foundation under NRF RF Award No. NRF-RF2013-08, the start-up funding from Nanyang Technological University (M4081137.070).

Author contribution

S. Z. conceived the experiments and prepared the samples. J. S. and S. Z. conducted the cathodoluminescence measurements. F. Liu did the Raman and photoluminescence measurements. The manuscript was written by S. Z., F. L., Z. L., N. Z., and H. J. F. H. J. Fan supervised the project. All authors participated in discussion of the data.

Additional information

Details of sample transfer, AFM, optical images, and more cathodoluminescence spectra.